Arabian Journal of Chemistry (2020) 13, 5312–5325

King Saud University

Arabian Journal of Chemistry

www.ksu.edu.sa
www.sciencedirect.com

ORIGINAL ARTICLE

Study of the adsorbent properties of nickel oxide for phenol depollution

Younes Dehmani *, Sadik Abouarnadasse

Laboratory of Chemistry/Biology Applied to the Environment, Faculty of Sciences, Moulay Ismaïl University, BP 11201-Zitoune, Meknes 50070, Morocco

Received 2 January 2020; accepted 10 March 2020
Available online 19 March 2020

KEYWORDS

Nickel oxide;
Phenol;
Adsorption;
Kinetic;
Thermodynamic;
Adsorption mechanism

Abstract Phenol and its derivatives are considered as dangerous pollutants due to these harmful effects on health and the environment. Treatment of the waters charged by these compounds by adsorption remains very important. For these reasons, this study was designed to prepare nickel oxide by precipitation method in order to remove these pollutants from aquatic environments. Indeed, structural and textural properties of this solid have been determined by various physico-chemical methods (X-ray diffraction, Fourier transform in the infrared, N2 adsorption/desorption (BET), ATD / ATG thermal analysis and scanning electron microscopy (SEM)). In addition, several adsorption tests were carried out in order to show the effectiveness of this solid for the elimination of phenol in aqueous solution and to determine the physicochemical parameters which affect adsorption. Our results have shown 5.29 $mg{\cdot}g^{-1}$ of adsorption capacity with 98% of yield. Furthermore, it was shown that adsorption process was endothermic. For the kinetic study, it was demonstrated that phenol adsorption on NiO follows the pseudo-second-order and the Langmuir model better adaptable for the isotherm of desorption. Moreover, thermodynamic study shows positive values of ΔS° (266.6 $JK^{-1}{\cdot}mol^{-1}$) suggesting a randomness increase of the solid/liquid interface. ΔH° (60.41 $kJ{\cdot}mol^{-1}$) was also positive confirming the endothermic nature of the adsorption processes. However, ΔG° ($kJ{\cdot}mol^{-1}$) was negative suggesting the spontaneity of the phenol adsorption. In summary, this work suggests that phenol adsorption on NiO was linked to the chemical adsorbate/adsorbent interactions.

1. Introduction

Phenol and its derivatives belong to the family of the volatile organic compounds, it is a pollutant that is widespread in many industrial effluents, such as the oil refining, the manufacture of leather and textile, the Steel Foundry and the manufacturing of olive oil (Slim et al., 2013). The strong ability of phenol to penetrate the skin and mucosal barriers and its effects on the nervous and cardiovascular system make him a

* Corresponding author.
E-mail address: dehmaniy@gmail.com (Y. Dehmani).
Peer review under responsibility of King Saud University.

ELSEVIER Production and hosting by Elsevier

https://doi.org/10.1016/j.arabjc.2020.03.010
1878-5352

very dangerous pollutant for human health (Ali et al., 2019; Abbasi, 2019).

Several studies conducted on the effect of phenol concentrated on the skin can cause severe skin lesions (Mandal and Das, 2019a). There are cases of poisoning death. Indeed, the accidental or intentional ingestion of a quantity of phenols (5–500 mg) is linked, frequently, with infants deaths. However, adult death can be caused following the ingestion of 1–32 g (H. Li et al., 2019; Jiang et al., 2002).

The presence of phenol in wastewater represents an important issue, related to toxicity to aquatic life and at concentrations of the order of the ppb (part per billion), enough to infuse the water smell and taste particularly unpleasant (Abbasi, 2019; Jiang et al., 2002). In addition, biological treatment of phenol at concentrations higher than 200 $mg{\cdot}L^{-1}$ is not possible due to the bactericidal effect of this compound. Without effect, predictable environmental concentration amounts to 7.73 $g{\cdot}L^{-1}$. This substance attacks mainly to the liver, kidneys, lungs and vascular system. No study could demonstrate its carcinogenic potential (Lütke et al., 2019; Liu et al., 2019).

Therefore, it is necessary to eliminate phenols from industrial wastewater before their release into the environment in which the flora and fauna are the main targets of these industrial effluents (Zif- et al., 2020). The elimination of phenol from the affluent represents a challenge for the scientific communities. Numerous techniques have been used to eliminate these toxic compounds prior to their release into the environment, with great interest for these pollutants recovery methods (Jin et al., 2014). In particular, catalytic oxidation, biological degradation, electrochemical oxidation, liquid-liquid extraction and membrane filtration (Lütke et al., 2019; Z. Li et al., 2019).

Among all of these methods of treatment, the adsorption of phenols on solid media such as activated carbon, clay and oxides of transition metals allows their removal in the water without the addition of chemicals (Awad et al., 2019; Giraldo and Moreno-Pirajan, 2014; Jiang et al., 2002, 2002, 2020; Ouallal et al., 2019; Yu et al., 2017).

Nickel oxide NiO is a functional material very important due to its electrical, structural, optical and catalytic properties. The latter has been used in several areas, namely the field of batteries (Mandal and Das, 2019a), the field of electrochemical capacitors (Rogozea et al., 2017), optical materials and in the field of catalysis (Mehraban et al., 2007).

The structural and textural material properties depend on the method of preparation of the latter, precursors and agent of precipitation. This oxide were widely used by various researchers in the adsorption of pollutants due to these promising properties in adsorption of propionic acid (El-Qanni et al., 2017), Cr (VI) (Behnajady and Bimeghdar, 2014), lead and cadmium (Mahmood et al., 2011; Li et al., 2016; Sheela and Nayaka, 2012), and malachite green dye (Abukhadra et al., 2019). The yield and capacity of this solid in the elimination of these pollutants and the absence of studies in the literature on adsorption of phenol on nickel oxide and the weak capacity of adsorption of phenol on several adsorbents mentioned in several works (Ba Mohammed et al., 2019; Cheng et al., 2015; Li et al., 2012; Mandal and Das, 2019b) have led us to test this solid in the elimination of phenol in aquatic environments.

In this work, we report the preparation of Nickel Oxide, and its use in the removal of phenol from aquatic environments. A structural and textural study by N_2 adsorption/desorption, Fourier Transform Infrared, X-ray diffraction, and scanning electron microscope was carried out. Phenol removal potential was evaluated under various working conditions (temperature, adsorbent mass, initial concentration, stirring speed and pH), kinetic and thermodynamic process study were carried out to determine the nature of the process. The interaction between the solid and the liquid was studied by the characterization after the adsorption of phenol. The most important part of this article is the study of the influence of the parameters of the nickel oxide particles and the calcination temperature on the adsorbed quantity.

2. Experimental

2.1. Preparation of the adsorbent

A mass of nickel nitrate dihydrate ($Ni(NO_3)_2$, 6 H_2O) was dissolved in a volume of distilled water. To this mixture we added, drop by drop (7 ml/min) 20 ml, a molar solution of ammonia (NH4OH). The resulting mixture was heated under constant stirring at 40 °C for 1 h and then filtered under vacuum. The resulting solid is washed several times with distilled water and dried overnight in an oven at 100 °C. The dried powder was charred at 200, 300, 400 and 500 °C for 3 h (Dehbi et al., 2019).

2.2. Characterization of oxide

***DRX*:** Diffraction of X-rays (*DRX*) diagrams were obtained using a diffractometer X – PERT MPD – PRO-powder for X-rays with a Monochromator to diffracted beam and CuKα radiation f (λ = 1.5406 Å). The voltage was 45 kV and the intensity was 40 mA. The angle 2θ was scanned between 4° and 30°, and the counting time was 2.0 s at each corner step (0.02°).

***FTIR*:** the Fourier transform infrared (*FTIR*) was carried out using a device (Shimadzu, JASCO 4100). In the range of 400 cm^{-1} to 4000 cm^{-1}.

SEM: the observation with the electron microscopy scanning (*SEM*) has the advantage to allow us to visualize surfaces. scanning electron microscope (*SEM*) images were obtained by a Brand EIF Quanta 200 device of a spectroscopy x-ray X (*EDX*).

BET: the textural property of solid was determined by the Adsorption/Desorption of N_2 in the temperature – 196 °C. In the calculations of the textural parameters using the BET (Bruner, Emet and T eller) method. The N_2 adsorption measurements were made using a Micromeritics ASAP 2010.

2.3. Determination of pH of the zero charge point pHzcp

The pH of zero charge point of nickel oxide is determined by following the consumption of important ions potential H^+ and OH^- (i.d.p) by the various sites of the surface. Indeed, we used the potentiometric method of volumetric titration. a titration cell is filled with 100 ml of electrolyte NaCl concentration 10^{-3}M and a mass of 625 mg of solid. Before starting the

titration procedure, it is essential to let set for one night to avoid the influence of the aging of the solid on the pH of the solution. The titling is as follows: 0.5 ml of HCl (0.5 M) is added to the solution of NaCl, then added 50 ul piecemeal of titrant concentration NaOH(0.2 M)in the cell by measuring the pH for each volume added. Blank titration is done in the same way as in the presence of the solid with the same concentration of electrolyte.

2.4. Adsorption experiments

The adsorption experiments were carried out at constant temperatures (T = 30, 40, 50, 60 °C). With stirring at 300 rpm for an adsorption period, a phenol solution (20 ml concentration defined $5*10^{-4}$M) connects to a mass of 0.1 g of NiO. The pH of the solutions in adsorption is adjusted to the needs of the experiences by NaOH or HCl. At the end of the reaction, the mixtures were filtered through a 0.45 μm Millipore filters are filtered, and analyzed by UV/visible. This a residual concentration was determined based on a calibration of the spectrometer UV unit curve / Visible at λ = 270 nm (Shimadzu UV-1240). The following equation was used to determine the quantity adsorbed.

$$q_t = \frac{C_0 - C_e}{m_{adsorbant}} \times V_{sol} \quad (1)$$

Qt is the adsorption capacity (mg / g), C0 is the initial concentration of phenol (mg / L), it is the residual concentration of phenol (mg / L), m is the mass of adsorbents used (g) and V is the volume of the solution (L) (Dabrowski et al., 2005).

Adsorption experiments were performed at least three times to examine the repeatability of the results and for verification of experimental data.

2.5. Isotherms and kinetics of adsorption

The study based on the time of adsorption of a compound on an adsorbent allows us to examine the influence of contact on its retention time and determine the kinetic law of reaction. In this view, two models have been used to describe the mechanism of the kinetics of adsorption of phenol on Nickel oxide, the pseudo-premier order (Eq. (2)) and the pseudo-second-order (Eq. (3)) (Li et al., 2012). The adsorption process takes place in several stages, including outreach, broadcasting intra-particulaire and effective adsorption on the surface. The intra-particular diffusion model (Eq. (4)) is used to adjust the experimental data in order to reveal the step speed control in the process of adsorption of phenol. Creating an isotherm of phenol on solid adsorption requires the determination of the amount adsorbed from the concentration in the solution to the balance at a selected temperature. The adsorption isotherm has been adjusted by the model of Freundlich and Langmuir model (Santos et al., 2019; Nthunya et al., 2019; Pakuła et al., 2007). The nonlinear equations of these models are grouped in Table 1:

The constants and variables indexed in Table 1 are, qe which represents the ability of adsorption at equilibrium ($mg{\cdot}g^{-1}$); q_t is the ability of adsorption at anytime ($mg{\cdot}g^{-1}$); and K_1 is the constant of kinetics of the first order of Lagergren (min^{-1}); K_2 is a constant kinetics of second-order of Lagergren ($g{\cdot}min^{-1}{\cdot}mg^{-1}$). Kid is the rate constantly of the intergranular diffusion equation ($mg{\cdot}g^{-1}{\cdot}min^{-1/2}$); and C is a constant related to the thickness of the layer limit ($g{\cdot}mg^{-1}{\cdot}min^{-1}$), it is the concentration of the solution at equilibrium ($mg{\cdot}L^{-1}$); q_e is the adsorption capacity of adsorbents for balance ($mg{\cdot}g^{-1}$); q_m is the theoretical ability of adsorption saturated with adsorbents ($mg{\cdot}g^{-1}$) and K_L, K_F respectively are the constants of Langmuir, Freundlich, and n corresponds to the intensity of adsorption between 1 and 0 (Ba Mohammed et al., 2019).

Table 1 Isothermal modules of adsorption.

Kinetic models		
Pseudo first order	$Ln(q_e - q_t) = Ln(q_e) - k_1 t$	(2)
Pseudo second order	$\frac{t}{q_e} = \frac{1}{q_e^2 k_2} + \frac{1}{q_e} t$	(3)
Weber and Morris	$q_t = k_{id}\sqrt{t} + C_i$	(4)
Isotherms models		
Langmuir	$q_e = \frac{q_m K_L C_e}{1 + K_L C_e}$	(5)
Freundlich	$q_e = K_F C_e^{1/n}$	(6)
Error Functions		
Standard deviation:	Δq (%)	

2.6. Adsorption thermodynamics

The values of the equilibrium constants K_e^0 of the phenol adsorption on the NiO were determined by the isothermal model constants (*KL* or *KF*). These values were used to calculate the thermodynamic parameters, $\Delta G°$ and $\Delta H°$ using the following equations (8).

$$K_e^0 = \frac{1000 * K * \text{moleculair weigth of adsorbate} * [\text{absorbate}]^0}{\gamma}$$

$$K_e^0 = 1000 * K * 94.11 * 1$$

$$\Delta G^0 = -RT\ln(K_e^0) \quad (8)$$

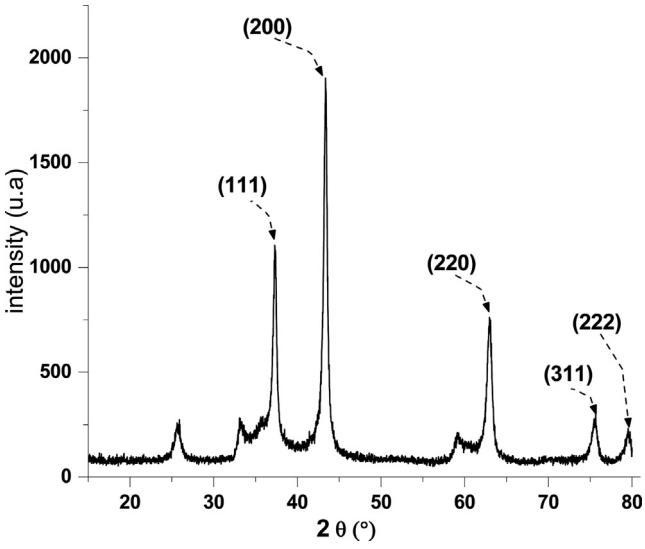

Fig. 1 Nickel oxide diffractogram.

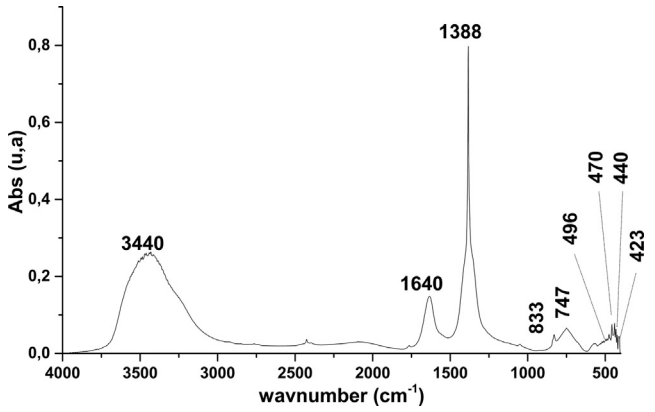

Fig. 2 FTIR spectra of NiO.

With $\ln(K_e^0) = -\frac{\Delta H}{RT} + \frac{\Delta S}{R}$

In these equations, ΔG° is the change in Gibbs free energy (kJ·mol^{-1}); ΔH° is the change in enthalpy (kJ·mol^{-1}); △S° is the change of enthalpy (J·K^{-1}·mol^{-1}); where K_e^0 is the thermodynamic equilibrium constant without dimension. K is the constant of the best adjusted isothermal model, γ is the activity coefficient and [adsorbate]° is the standard concentration of the adsorbate which, by definition, is 1 mol L^{-1} (8.314 J mol^{-1}·K^{-1}) (Lima et al., 2019a; Lima et al., 2019b).

3. Result and discussions

3.1. X-ray diffraction

The diffractogram of the Nickel oxide (Fig. 1) shows peaks of diffraction at 2θ = 37.2°, 43.3, 62.9°, 75.4°, and 79.4° could be assigned to crystalline plans (1 1 1), (2 0 0), (2 2 0), (3 1 1) and (2 2 2). All the reflections can be indexed in phase cubic centered (fcc) with a constant in the network (a): 4.175 A (space group Fm 3 h m [2 2 5]) (Khaleed et al., 2017), which is consistent with standard data (card JCPDS No. 47-1049). The sharpness and intensity of the peaks show the good crystalline nature of the prepared sample. No pics due to the or $Ni(OH)_2$ were found from XRD, indicating that neither $Ni(OH)_2$ was completely broken down into NiO at 500 °C pendant 3 h, (Behnajady and Bimeghdar, 2014; Saleh et al., 2019).

3.2. Fourier transform infrared

The spectrum corresponding to the charred NiO sample (Fig. 2) shows bands located at 833, 747, 496,470, 440 and 423 cm^{-1} characterizing NiO. We note also the presence of a strip to 1388 cm^{-1} assigned to the vibration of CO_2 adsorbed form and which comes from the ambient air. On the same spectrum, we note the presence of a band to 1640 and 3440 cm^{-1} these bands correspond to the vibration of the hydroxyl of the water (Khaleed et al., 2017;Lu and Kawamoto, 2013).

3.3. Adsorption and desorption of N2 BET

To estimate the surface microstructures NiO, isotherms of adsorption / desorption of nitrogen were carried out, and the distribution of pore size, respectively, is shown in (Fig. 3). According to the IUPAC, the isotherm can be classified as type IV and behavior of hysteresis H4. The structural results are grouped in Table 2 (Alali et al., 2017; Emamdoust and Farjami Shayesteh, 2018).

3.4. Scanning electron microscopy SEM

Nickel oxide *SEM* analysis was conducted to obtain information on their morphologies. From a visual observation from

Table 2 Textural properties of NiO.

Surface area ($m^2 \cdot g^{-1}$)	Volume ($cm^3 \cdot g^{-1}$)	Diameter of the pore (Å)
3.9310	0.012476	126.9463

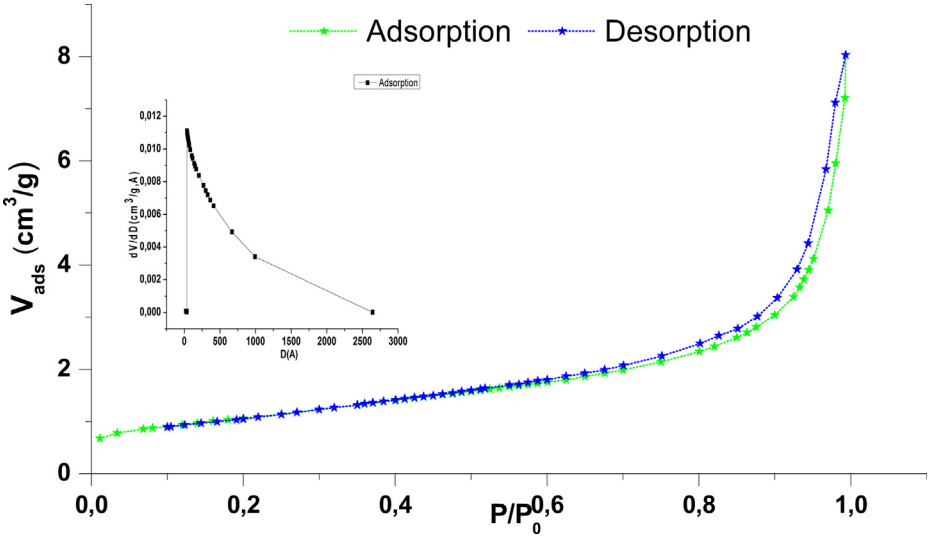

Fig. 3 Adsorption/Desorption of N2 on NiO.

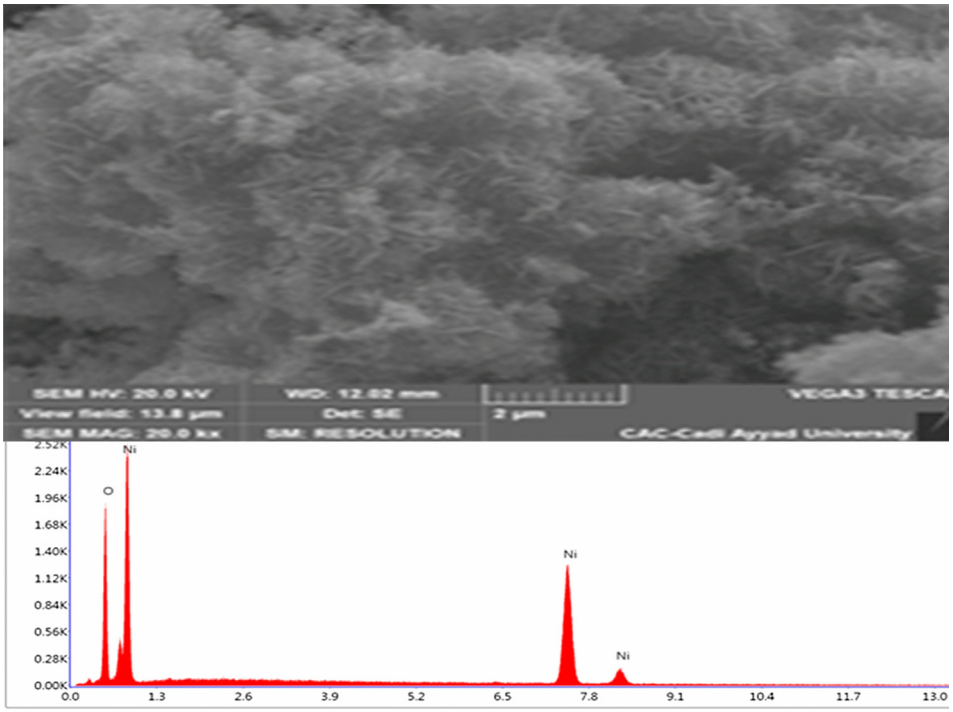

Fig. 4 Scanning electron microscope image.

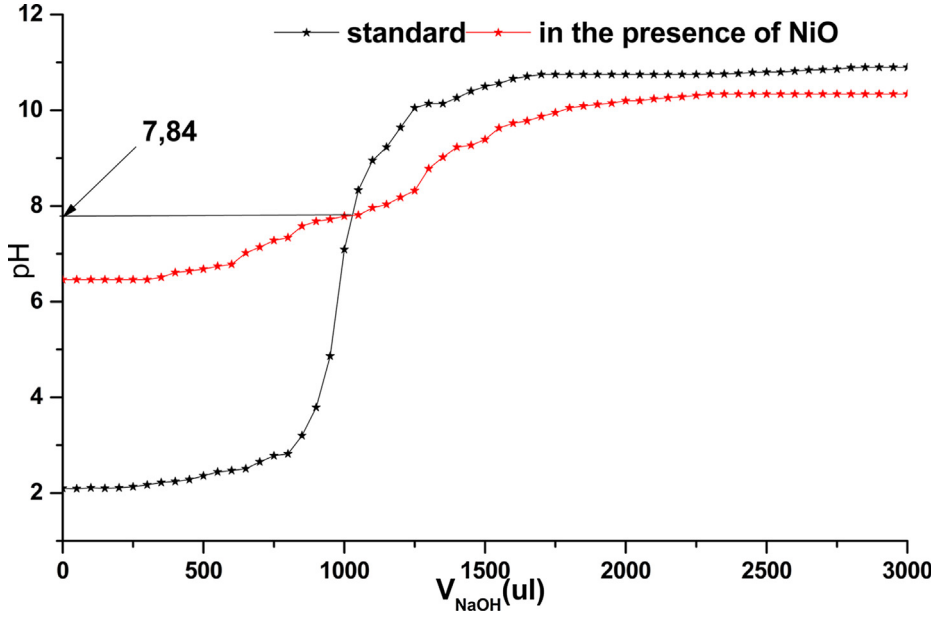

Fig. 5 Variation of pH based on V_{NaOH}.

Fig. 4, we can highlight the following: the pure surface of NiO Nanopowders consist of grains of irregular shape merged with each other. The *SEM* image shows that its surface is made of lamellar fibers with distinct sticks, Spectra *EDX* (Fig. 4) confirmed the presence of NiO elements. The atomic percentage of elements composition Ni and O is respectively equal to 43.3% and 56.7% (Kumar et al., 2018; Yang et al., 2018).

3.5. pH of the zero charge point pHzcp

The determination of the pH of the zero charge point is very important in the adsorption process that gives us information on the nature of the dominant sites on the solid surface. The results showed that the variation of pH was dependent to the volume of added NaOH (Fig. 5).

The pHpzc or pH of the point of zero charge corresponds to the pH value for which the net charge of the surface of the NiO is zero. This parameter is very important in adsorption phenomena, especially when electrostatic forces are involved in the mechanisms. The pH of point load zero (pHpcn) oxide NiO is 7.84, this value shows that the surface is positive in the case of pH < 7.84 and negative in the case of pH > 7.84. In this work, adsorption of phenol was more pronounced in the case of positive charges in the pH < pHpcn (7.84) of solid.

3.6. Adsorption of phenol

3.6.1. Kinetics of adsorption

The kinetics of adsorption of phenol on the nickel oxide at different temperatures is shown in Fig. 6. Adsorption was very fast when the contact duration does not exceed 3 h for all working temperatures. Indeed, the amounts of adsorption for oxide were 3.58, 4.50, and 5.29 $mg{\cdot}g^{-1}$ for 30, 40, and 50 °C respectively. So we can conclude that the adsorbed amount increased with manner dependent on the temperature's increase. This may suggest that the process is endothermic (Makrigianni et al., 2015; Luo et al., 2015). This quantity adsorbed and the removal efficiency of this pollutant is very important in comparison with other works of literature (Ioannou and Simitzis, 2009; Abdelkreem, 2013; Kong et al., 2020), this property is essentially dependent on the structural and textural properties of this solid.

The experimental data are used by several ways to determine the model of the kinetics of adsorption of phenol on Nickel oxide. In the case of liquid/solid contact, several models have been proposed by Kannan et al, (equ2) and Ho and Coll (equ3) and broadcast intraparticulaire (equ4) model can be applied to explore the progress of adsorption (Sheela and Nayaka, 2012). Modeling of experimental data by linear forms of kinetic models is presented in Fig. 7 (Hank et al., 2014).

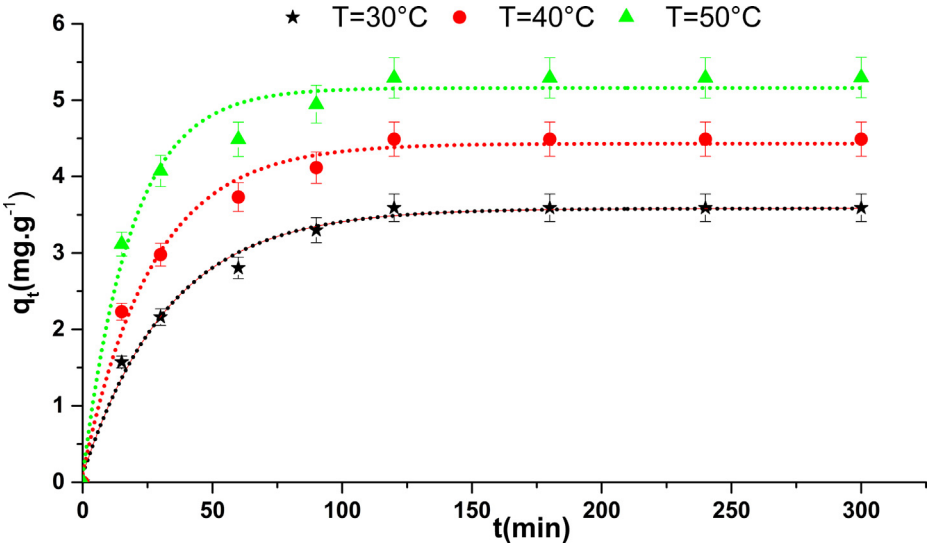

Fig. 6 Kinetics of adsorption of phenol on NiO.

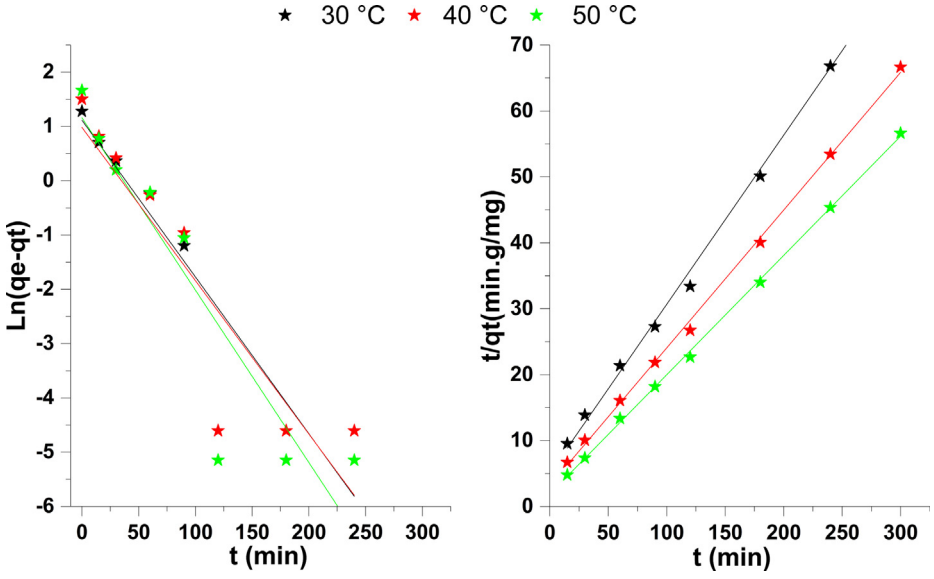

Fig. 7 Modeling of the kinetics of adsorption of phenol.

According to Table 3, the correlation coefficients calculated from modeling the adsorption kinetics of phenol on nickel oxide are very close to unity for the pseudo-second-order kinetic model than the pseudo-First order model and the theoretical adsorption capacities are closer to those obtained experimentally for the model pseudo-second order. This indicates that the experimental results of adsorption of phenol on the adsorbent are well described by the second-order kinetic model. The low values of the kinetic constant k_2 showed that the adsorption was rapid (Pirmoradi et al., 2017).

Fig. 8 shows the variation of qt in function $t^{1/2}$. In this Figure, it should be noted that the adsorption process is divided into two stages, indicating that the complex adsorption process is controlled by several mechanisms. The original intercept values C are not equal to zero according to the values of Table 4, which shows that the step of controlling the adsorption rate is not only the spread of the pores but also the dissemination of the outer layer.

We can conclude that this model has two steps in the adsorption of phenol on the oxide NiO, the first step has been attributed to the interactions of the molecules of phenol with the sites available on the surface of NiO, while the second stage is penetration gradually of the adsorbent in the pores of the adsorbents in which broadcasting intraparticule becomes slower due to her weaken concentration (Bhatnagar et al., 2010; Gerçel and Gerçel, 2007).

The values of k_{id}, C and R^2 are given in Table 4. Indeed, intraparticular diffusion model showed a better representation of the data when compared with the pseudo-first-order model. the R^2 values of the intraparticular distribution model were lower, suggesting that the removal of phenol from an aqueous solution should be closely related to the initial phenol concentration.

3.6.2. Calculation of activation energy

The adsorption activation energy of phenol on NiO can be calculated from the kinetics data, performed at working temperatures. Knowing the values of the second-order rate constants gives a possibility of calculating Ea using the linearization of the following Arrhenius relation:

$$Lnk_2 = LnA - \frac{E_a}{RT}$$

Table 3 Kinetic parameters for adsorption of phenol on NiO.

T °C	qads ($mg{\cdot}g^{-1}$)	Lagergren pseudo First order				Ho and Col pseudo second-order			
		K (min^{-1})	qe ($mg{\cdot}g^{-1}$)	R^2	Δq(%)	K_2 ($g{\cdot}mg^{-1}{\cdot}min^{-1}$)	Qe ($mg{\cdot}g^{-1}$)	R^2	Δq(%)
30	3.58	0.031	3.575	0.98	0,6751	0.010	4.027	0.999	0.844
40	4.50	0.039	4.424	0.98	0.6004	0.011	4.903	0.995	0.496
50	5.29	12.244	4.724	0.818	0.5879	0.015	5.591	0.996	0.316

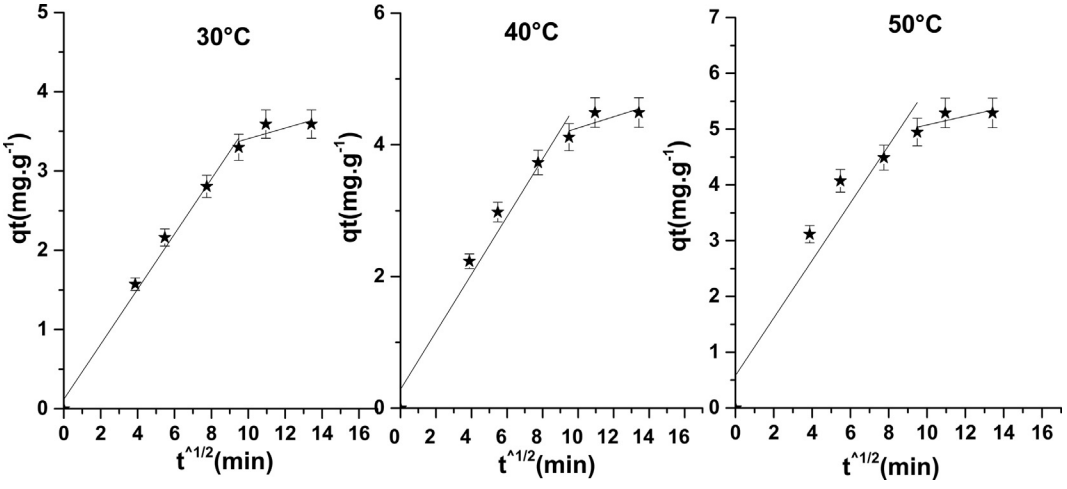

Fig. 8 Intraparticular diffusion model of phenol on NiO.

Table 4 Parameters of the intraparticle scattering model.

T (°C)	Step 1			Step 1		
	K_1d ($mg{\cdot}g^{-1}{\cdot}min^{-1}$)	C1	R^2	K_2d ($mg{\cdot}g^{-1}{\cdot}min^{-1}$)	C_2	R^2
30	0.3475	0.11	0.9955	0.6668	2.74	0.7846
40	0.43	0.28	0.981	0.085	3.40	0.7846
50	0.58	0.51	0.989	0.078	4.29	0.786

with: k2 ($g \cdot mg^{-1} \cdot min^{-1}$): constant speed of the pseudo-second-order; A (min^{-1}): pre-exponential factor or frequency factor; Ea ($kJ \cdot mol^{-1}$): activation energy; R (8,314 $Joule \cdot mole^{-1} \cdot K^{-1}$): perfect gas constant; T (K): adsorption temperature.

Fig. 9 shows obtaining a right according to the Arrhenius relationship. The energy of activation deducted from the slope of this line is Ea = 34.77 $kJ \cdot mole^{-1}$. This last value indicates that the adsorption process and fast with a low potential energy constraint

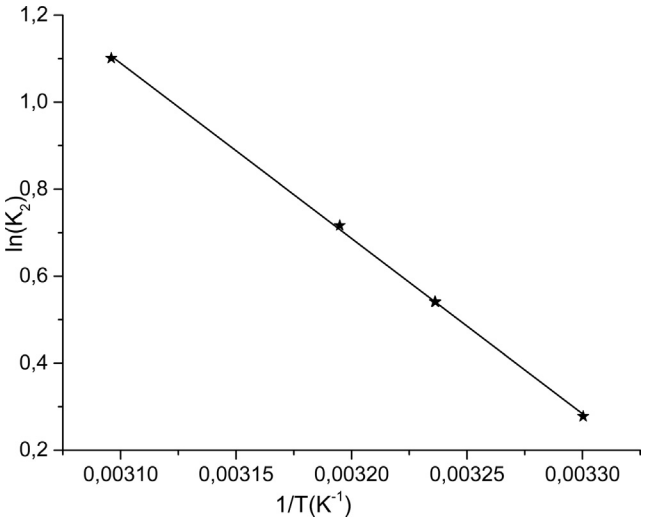

Fig. 9 Variation of Ln (k_2) according to $1/T(K^{-1})$.

3.6.3. Phenol adsorption isotherm

The adsorption isotherm models are shown in Fig. 10. the values of the squared correlation coefficients obtained show that they are higher in the case of the Langmuir model (Table 5), and therefore in that of phenol. The adsorption on NiO is done on energetically homogeneous sites probably forming a monolayer, which reinforces the validity of the Langmuir model based on the absence of interactions between entities adsorbed on sites of a similar nature. An important remark on the values of K_F and K_L an increase as a function of the temperature which confirms the endothermic nature of the adsorption phenomenon

3.6.4. Thermodynamic study of adsorption of phenol

Adsorption is a phenomenon that can be endothermic or exothermic by absorbent material and the nature of the adsorbed molecules. The study of the effect of temperature on adsorption has been performed to determine the thermodynamic settings such as the free energy change (ΔG °), the variation of enthalpy (ΔH°) and the variation of entropy (ΔS °). Eq. (8) was used for this analysis, By tracing the equation of Van't Hoff, ln (K_e^0) in terms of 1/T (Fig. 11), it determines the values of the previous sizes that are listed in Table 6

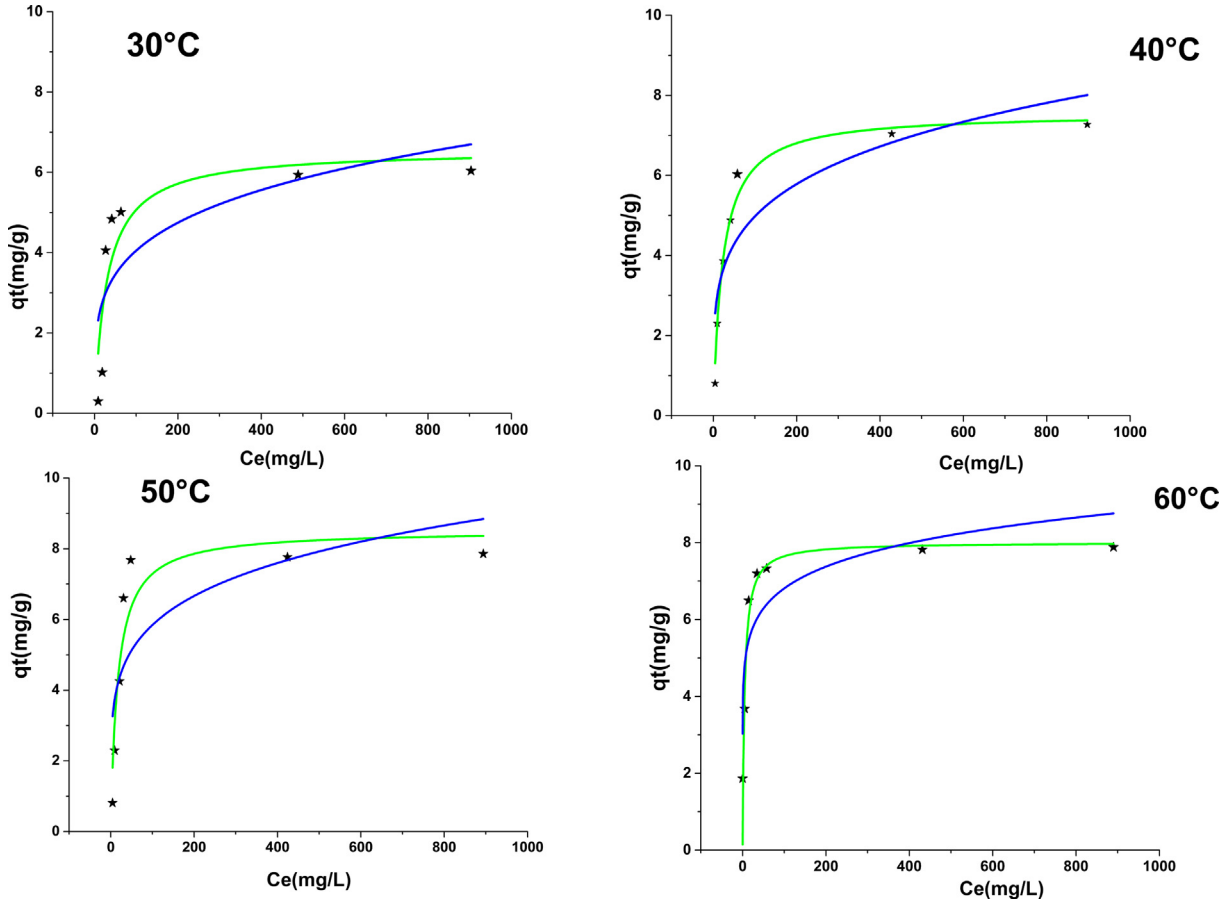

Fig. 10 Isotherm adsorption of phenol on NiO at different temperatures with nonlinear regression of Langmuir and Freundlich models.

Table 5 The model parameters for adsorption of phenol on NiO.

T (°C)	Langmuir			Freundlich		
	R^2	K_L ($L{\cdot}mg^{-1}$)	Q_m ($mg{\cdot}g^{-1}$)	R^2	K_F ($mg{\cdot}g^{-1}$)	1/n
30	0.962	0.02	6.558	0.73	1.41	0.22
40	0.985	0.045	7.557	0.797	1.84	0.185
50	0.95	0.059	8.519	0.616	2.448	0.189
60	0.96	0.2113	8.52	0.77	3.80	0.13

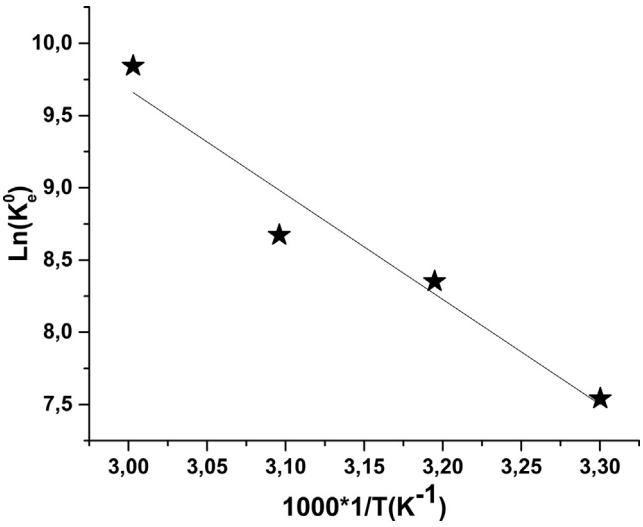

Fig. 11 Variation of Ln (K_e^0) in terms of 1/T.

Table 6 Thermodynamic parameters for adsorption of phenol on NiO.

T (°C)	ΔS° ($J.K^{-1}{\cdot}mol^{-1}$)	ΔH° ($kJ{\cdot}mol^{-1}$)	ΔG° ($kJ{\cdot}mol^{-1}$)
30	266.6	60.41	−20.19
40			−22.85
50			−25.51
60			−28.17

(Gupta and Balomajumder, 2015). The adsorption isotherm of phenol on nickel oxide is written by the Langumiur model so the equilibrium constant is equal to:

$$K_e^0 = 1000 * K_L * 94.11 * 1$$

Negative values for the free energy ΔG indicate the feasibility of the process of adsorption and its spontaneous nature. This can also be noted from the Table, that the increase in temperature is accompanied by a decrease in the values of free energy and an increase in the capacity of adsorption. We can say that a rise in temperature leads to a spacing between particles of oxide, and therefore a greater diffusion of molecules of phenol or the redistribution of energy between the phenol and Nickel oxide (Marques et al., 2015).

Positive values of enthalpy ΔH for the retention of the phenol process confirm the endothermic process nature, while positive values of entropy ΔS reflect the good affinity of phenol to the oxide (Mandal and Das, 2019a; Al-Malack and Dauda, 2017).

3.6.5. Initial concentration effect

Fig. 12 shows the evolution of the adsorbed quantity of phenol by nickel oxide according to the contact time with different initial concentrations (10^{-3}, 5 * 10^{-4}, 10^{-4} M). it was seen that the quantity of adsorbent attached to the material increases with concentration. In fact, the increase in concentration induced the elevation of the driving force of the concentration gradient, thus increasing the spread of the particles in solution across the surface of the adsorbent (Ardejani et al., 2008). The results of elimination of the phenol on the Nickel oxide shows an important efficiency, with returns exceeding 95%, these results offer a promising future in the use of this solid in the treatment of waste water of the tanneries and in the depopulation of the rejections oil mills.

3.6.6. Effect of pH on the adsorption of phenol

The increase in the pH slightly diminishes the ability of adsorption of phenol. Indeed adsorption to balance capabilities are respectively 4.49 $mg{\cdot}g^{-1}$ for a pH = 3, 5, and 1, 45 $mg{\cdot}g^{-1}$ mg for a pH = 10, 7, this can be explained by the fact that to the basic state (pH > pHpcn), the dominant load in the surface of the adsorbent is negative which reduces the adsorption of the phenolates carrying the same load (Hank et al., 2014; Wang et al., 2015). The acidic state, the positive charge is dominant on the surface of the adsorbent and thus a significantly high electrostatic attraction between the positive charges of the surface of the adsorbent and the negative charges of the phenolates formed which promotes the adsorption (Abdelwahab and Amin, 2013; Lütke et al., 2019).

3.6.7. Effect of the mass of adsorbent

These curves (Fig.14) show that the adsorbed quantity decreases with mass (Fig. 13). Indeed, for a mass of 0.1 g,

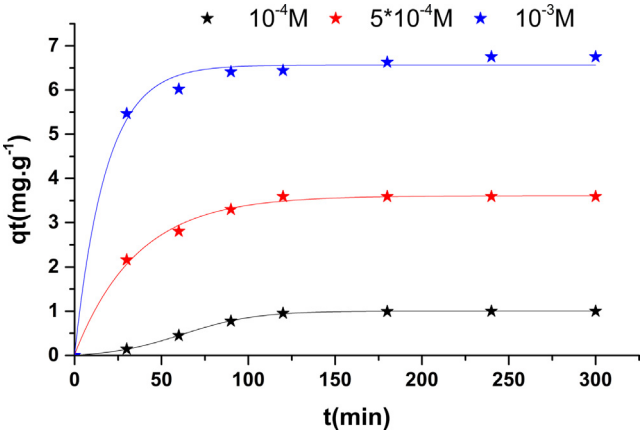

Fig. 12 Initial concentration effect.

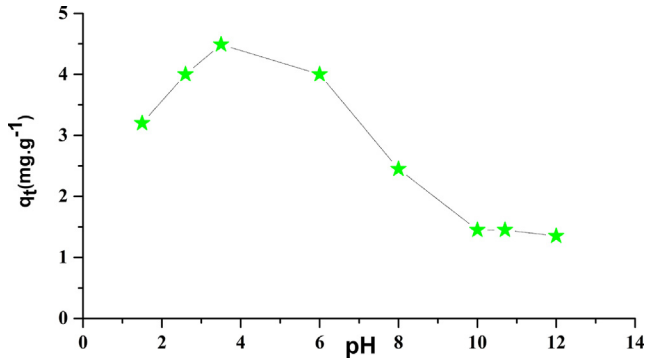

Fig. 13 pH effect.

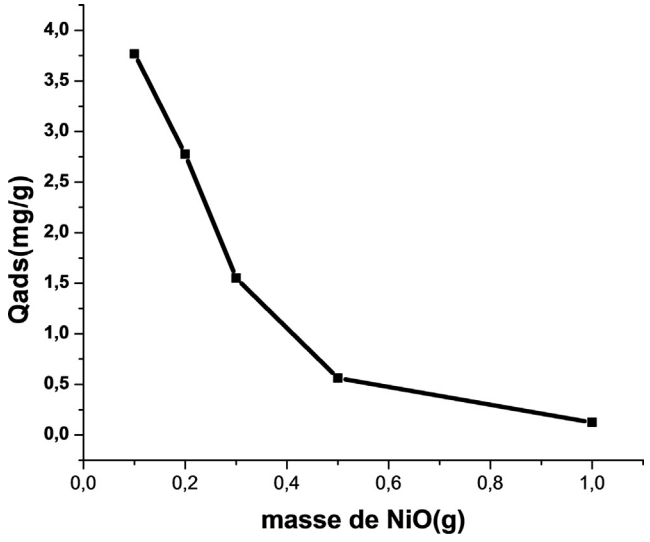

Fig. 14 The mass effect of adsorbent on the adsorption of phenol.

the adsorbed amount of phenol is of the order of 3.76 mg·g^{-1}, while for a mass of 1 g is 0.1247 mg·g^{-1}. These results can be explained by the fact that the adsorption sites are more accessible to the weak masses of nickel oxide (Mandal and Das, 2019a).

3.6.8. Stirring speed effect

According to the Fig. 15, it can be observed that the adsorbed quantity varies according to the stirring speed until it reaches optimum speed.

3.6.9. Effect of calcination temperature

Of after the Fig. 16 it can be seen that the quantity adsorbed by the solid calcined at 200 °C is higher in comparison to the other quantities adsorbed by other solid calcined at 300 °C, 400 °C, and 500 °C. These results can be explained by the structural and textural effect on the solids. in short, the calcination temperature increases the crystallinity of solid increases interiane a diminution of the specific surface

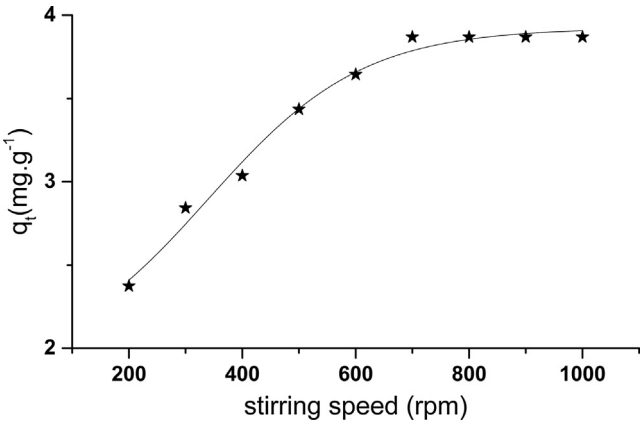

Fig. 15 Effect of the stirring speed.

Diagrams of rays X of Nio (Fig. 17) have indicated that they have a cubic structure. All the reflections can be indexed in phase NiO centered cubic (fcc) with a constant in the network (a): 4.175 A (space group Fm 3 h m [2 2 5]) (Khaleed et al., 2017). Note that we can attract the existence of peaks or $(OH)_2$ in the solid calcined at 200 °C. from the Scherrer relation (N) we can determine the particle diameter of the solids. The average grain sizes (d) of the films were evaluated (Behnajady and Bimeghdar, 2014).

$$d = \frac{0.94 * \lambda}{\cos(\theta) * B}$$

λ , θ and B are the wavelength of x-rays (1.54 (A), the corner of Bragg diffraction and the width of stripe to half the maximum of (0-0-2) maximum respectively around 38.6 and 43.28°. The average size of grain of our samples is 15.53, 16.41, 26.32, 35.5 nm respectively for annealed samples at 200 °C, 300 °C, 400 °C and 500 °C, which indicates that the size of the particles increases with the increase of annealing. We conclude that the quantity adsorbed is poor according to the diameter of particle more calcination temperature increases, the larger the diameter of particle increases more the quantity adsorbed is reduced. the results of this effect on the quantity adsorbed and the efficiency of elimination of this solid can justify the mechanism for fixing phenol molecules on the solid

3.6.10. Mechanism of adsorption of phenol

a. Etude par *FTIR*

In order to understand the mechanism of phenol adsorption on nickel oxide, solid FTIR analyses were performed before and after contact with the phenol solution. The comparison of the NiO FTIR spectra before and after the phenol adsorption (Fig. 18) shows no appearance and disappearance of the bands in the virgin solid spectrum. The fact observed is the change in the intensity of certain absorption bands. Indeed, the bands characterizing the vibration of the OH hydroxyl groups (3436, 1633 and 1338 cm^{-1}) show a significant decrease in intensity as a function of the reaction time, this decrease in the OH bands shows that the fixation of phenol

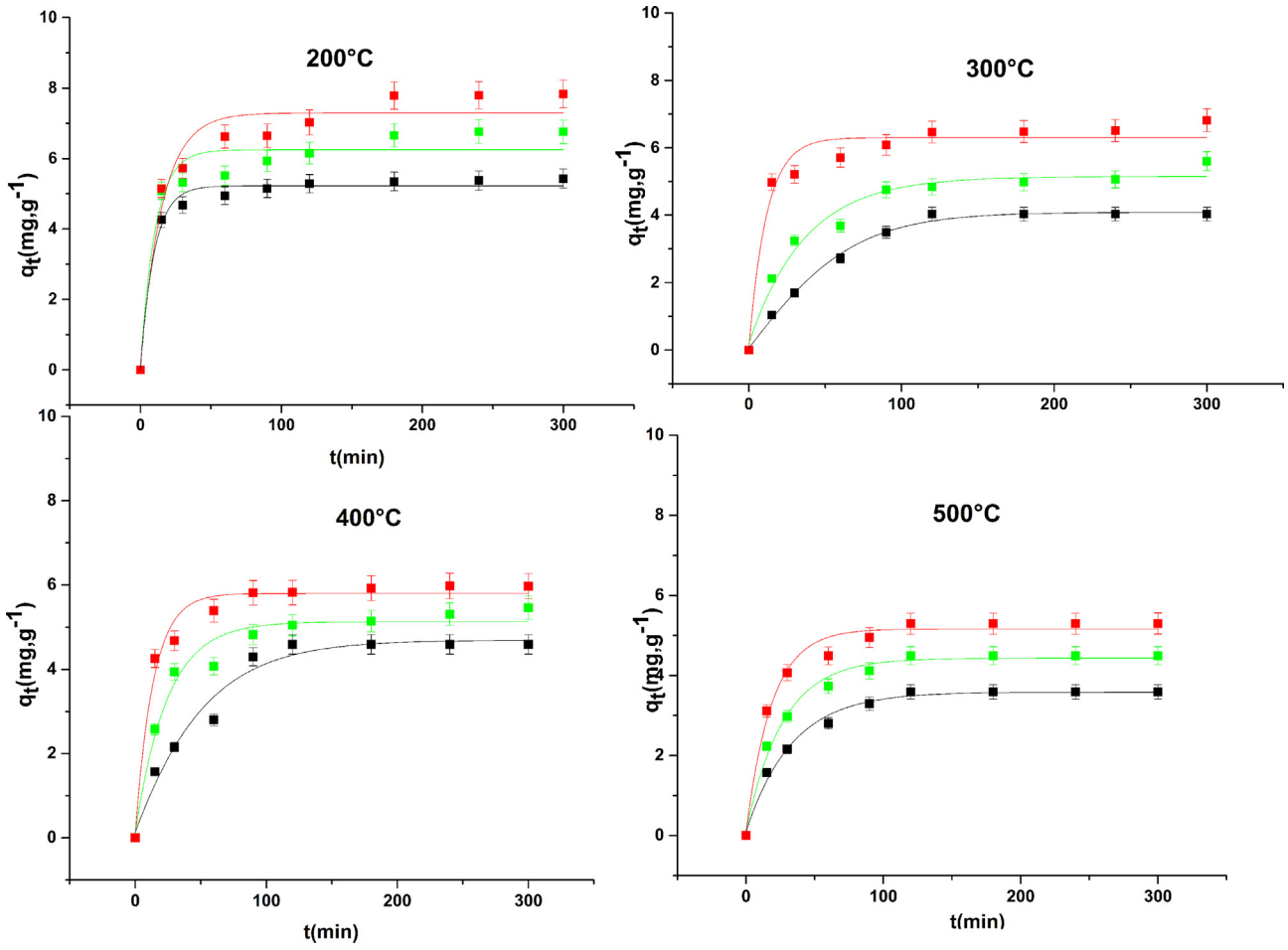

Fig. 16 Effect of calcination temperature on adsorption.

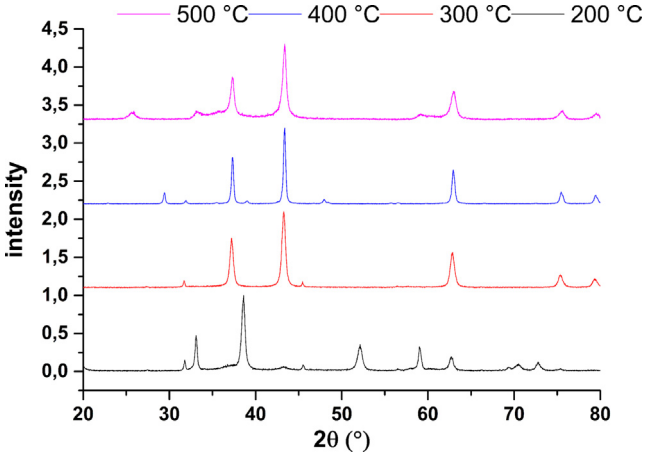

Fig. 17 XRD pattern of NiO at different calcination temperature.

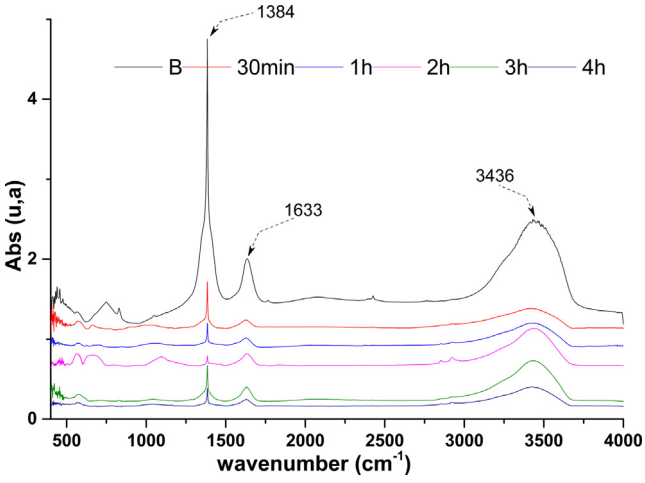

Fig. 18 FTIR spectra of NiO before and after adsorption.

ce do this in a way of catalyzed fission of the OH group of the hydroxyl and an adsorbed phenoxy radical (Jiang et al., 2020).

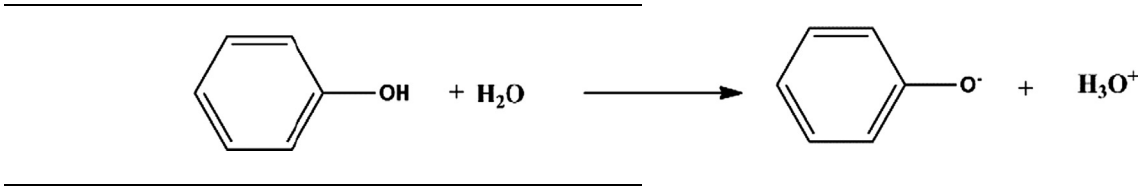

This indicates that the phenol molecules interact with the oxygen of the oxide groups and OH phenol groups, indicating that the phenolate ions were adsorbed on the NiO particles by weak bonds, by chemical interaction which is in agreement with the works of Seyedehsara and these collaborators (Mosallanejad et al., 2016).

b. XRD study

Fig. 19 shows the XRD profiles of Nickel Oxide before and after the adsorption of phenol. It can be noted that there is a disappearance of the main lines of the adsorbent 12.87, 25.89 and 33.07° with the conservation of the main lines after heat treatment of solid after the adsorption is observed the crystal structure of oxide before contact. It can be concluded that the fixation of the phenol molecule on nickel oxide is done at specific sites. The structural change of nickel oxide after the adsorption of phenol confirms that there are specific interactions between the adsorbate and the adsorbent.

Several mechanisms such as hydrophobic interaction, the hydrogen bond, and electrostatic interaction may be involved in the adsorption of phenol (Kong et al., 2020). In our case we can talk about three stages of the reaction of adsorption. First, we know that the State acid, the positive charge is dominant on the surface of the adsorbent and thus a significantly high electrostatic attraction between the positive charges of the surface of the adsorbent and negative charges of phenolates formed (1).

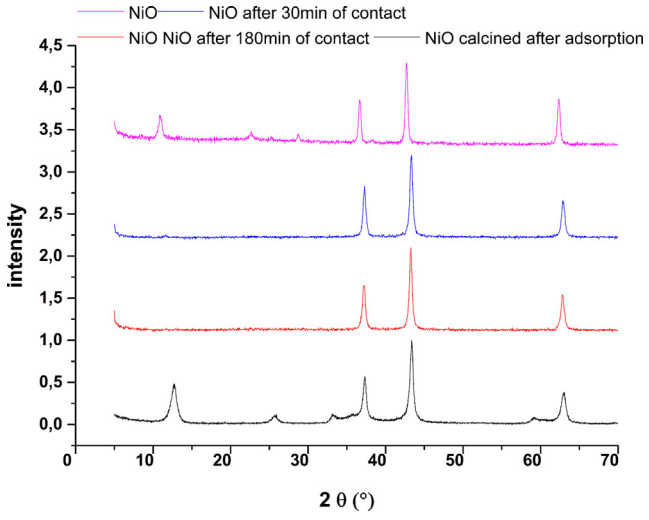

Fig. 19 NiO diffractograms before and after adsorption.

On the other hand, dissociated phenolic anions tend to interact with cations on the external surface of the oxide by interaction. The characterization data by infrared to transform Fourier after adsorption showed a signficative decrease in the intensities of the hydroxyl carterise bands which confirms the clearance between OH and a phenoxy (phenolate) by the hydrogenated layer. in addition, the results of the effect of the calcination temperature on the adsorption quantity show a significant increase with the decrease in temperature (effect of solid OH). The KF values (Freundlich constant) (Table 3) are increased when the temperature increases from 30 °C to 60 °C, in addition, the value $\Delta H = 60.41$ Kj / mole indicating that the phenol adsorption processes involve a reaction endothermic and chemical in nature. We can conclude from the results of the structural characterizations (DRX, FTIR) and experimental data of isothermal adsorption kinetics that the mechanism proposed in this system of adsorption of phenol on nickel oxide is i, chemical teractions between NiO and phenol.

4. Conclusion

In conclusion, the nickel oxide prepared by the precipitation method showed an efficiency for the recovery of phenol. The adsorption was very fast with a time not exceeding 3 h and an increase in the amount adsorbed with temperature, kinetically follows the pseudo-second-order model, with an activation energy of 34.77 kj·mol^{-1}. The isothermal adsorption of phenol on NiO was written by the Langmuir model. The thermodynamic results confirmed spontaneous and favorable adsorption of phenol in NiO. The results of the structural characterizations DRX, FTIR before and after the adsorption and the experimental data of the isotherm and the adsorption kinetics showed that the mechanism proposed in this system of adsorption of phenol on nickel oxide is chemical.

Funding

This research did not receive any specific grant from funding agencies in the public, commercial, or not-for-profit sectors.

References

Abbasi, A., 2019. Adsorption of phenol, hydrazine and thiophene on stanene monolayers: a computational investigation. Synth. Met. 247, 26–36. https://doi.org/10.1016/j.synthmet.2018.11.012.

Abdelkreem, M., 2013. Adsorption of phenol from industrial wastewater using olive mill waste. APCBEE Procedia 5, 349–357. https://doi.org/10.1016/j.apcbee.2013.05.060.

Abdelwahab, O., Amin, N.K., 2013. Adsorption of phenol from aqueous solutions by Luffa cylindrica fibers: Kinetics, isotherm and thermodynamic studies. Egypt. J. Aquat. Res. 39, 215–223. https://doi.org/10.1016/j.ejar.2013.12.011.

Abukhadra, M.R., Adel, M., Rabie, A.M., Ahmed, S.A., 2019. Surface decoration of diatomite by Ni / NiO nanoparticles as hybrid composite of enhanced adsorption properties for malachite green dye and hexavalent chromium. Colloids Surf. A 577, 583–593. https://doi.org/10.1016/j.colsurfa.2019.06.018.

Al-Malack, M.H., Dauda, M., 2017. Competitive adsorption of cadmium and phenol on activated carbon produced from municipal sludge. J. Environ. Chem. Eng. 5, 2718–2729. https://doi.org/10.1016/j.jece.2017.05.027.

Alali, K.T., Liu, T., Liu, J., Liu, Q., Fertassi, M.A., Li, Z., Wang, J., 2017. Preparation and characterization of ZnO/CoNiO2hollow nanofibers by electrospinning method with enhanced gas sensing properties. J. Alloy. Compd. 702, 20–30. https://doi.org/10.1016/j.jallcom.2017.01.167.

Ali, S.N.F., Al-busa, S., Al-lawati, H.A.J., 2019. Journal of Environmental Chemical Engineering Adsorption of chlorpheniramine and ibuprofen on surface functionalized activated carbons from deionized water and spiked hospital wastewater 7. https://doi.org/10.1016/j.jece.2018.102860.

Ardejani, F.D., Badii, K., Limaee, N.Y., Shafaei, S.Z., Mirhabibi, A. R., 2008. Adsorption of Direct Red 80 dye from aqueous solution onto almond shells: Effect of pH, initial concentration and shell type 151, 730–737. https://doi.org/10.1016/j.jhazmat.2007.06.048.

Awad, A.M., Shaikh, S.M.R., Jalab, R., Gulied, M.H., Nasser, M.S., Benamor, A., Adham, S., 2019. Adsorption of organic pollutants by natural and modified clays: a comprehensive review. Sep. Purif. Technol. 228, 115719. https://doi.org/10.1016/j.seppur.2019.115719.

Ba Mohammed, B., Yamni, K., Tijani, N., Alrashdi, A.A., Zouihri, H., Dehmani, Y., Chung, I.-M., Kim, S.-H., Lgaz, H., 2019. Adsorptive removal of phenol using faujasite-type Y zeolite: Adsorption isotherms, kinetics and grand canonical Monte Carlo simulation studies. J. Mol. Liq. 296, 111997. https://doi.org/10.1016/j.molliq.2019.111997.

Behnajady, M.A., Bimeghdar, S., 2014. Synthesis of mesoporous NiO nanoparticles and their application in the adsorption of Cr (VI). Chem. Eng. J. 239, 105–113. https://doi.org/10.1016/j.cej.2013.10.102.

Bhatnagar, A., Minocha, A.K., Sillanpää, M., 2010. Adsorptive removal of cobalt from aqueous solution by utilizing lemon peel as biosorbent. Biochem. Eng. J. 48, 181–186. https://doi.org/10.1016/j.bej.2009.10.005.

Cheng, W.P., Gao, W., Cui, X., Ma, J.H., Li, R.F., 2015. Phenol adsorption equilibrium and kinetics on zeolite X/activated carbon composite. J. Taiwan Inst. Chem. Eng. 62, 192–198. https://doi.org/10.1016/j.jtice.2016.02.004.

Dabrowski, A., Podkościelny, P., Hubicki, Z., Barczak, M., 2005. Adsorption of phenolic compounds by activated carbon – A critical review. Chemosphere 58, 1049–1070. https://doi.org/10.1016/j.chemosphere.2004.09.067.

Dehbi, A., Dehmani, Y., Omari, H., Lammini, A., Elazhari, K., Abdallaoui, A., 2019. Hematite iron oxide nanoparticles (α-Fe2O3): synthesis and modelling adsorption of malachite green. J. Environ. Chem. Eng. 103394. https://doi.org/10.1016/j.jece.2019.103394.

El-Qanni, A., Nassar, N.N., Vitale, G., 2017. A combined experimental and computational modeling study on adsorption of propionic acid onto silica-embedded NiO/MgO nanoparticles. Chem. Eng. J. 327, 666–677. https://doi.org/10.1016/j.cej.2017.06.126.

Emamdoust, A., Farjami Shayesteh, S., 2018. Surface and electrochemical properties of flower-like Cu-NiO compounds. J. Alloy. Compd. 738, 432–439. https://doi.org/10.1016/j.jallcom.2017.12.144.

Gerçel, Ö., Gerçel, H.F., 2007. Adsorption of lead(II) ions from aqueous solutions by activated carbon prepared from biomass plant material of Euphorbia rigida. Chem. Eng. J. 132, 289–297. https://doi.org/10.1016/j.cej.2007.01.010.

Giraldo, L., Moreno-Pirajan, J.C., 2014. Study of adsorption of phenol on activated carbons obtained from eggshells. J. Anal. Appl. Pyrolysis 106, 41–47. https://doi.org/10.1016/j.jaap.2013.12.007.

Gupta, A., Balomajumder, C., 2015. Journal of environmental chemical engineering simultaneous adsorption of Cr (VI) and phenol onto tea waste biomass from binary mixture: Multicomponent adsorption, thermodynamic and kinetic study. Biochem. Pharmacol. 3, 785–796. https://doi.org/10.1016/j.jece.2015.03.003.

Hank, D., Azi, Z., Ait Hocine, S., Chaalal, O., Hellal, A., 2014. Optimization of phenol adsorption onto bentonite by factorial design methodology. J. Ind. Eng. Chem. 20, 2256–2263. https://doi.org/10.1016/j.jiec.2013.09.058.

Ioannou, Z., Simitzis, J., 2009. Adsorption kinetics of phenol and 3-nitrophenol from aqueous solutions on conventional and novel carbons. J. Hazard. Mater. 171, 954–964. https://doi.org/10.1016/j.jhazmat.2009.06.098.

Jiang, J.Q., Cooper, C., Ouki, S., 2002. Comparison of modified montmorillonite adsorbents Part I: preparation, characterization and phenol adsorption. Chemosphere 47, 711–716. https://doi.org/10.1016/S0045-6535(02)00011-5.

Jiang, N., Shang, R., Heijman, S.G.J., Rietveld, L.C., 2020. Adsorption of triclosan, trichlorophenol and phenol by high-silica zeolites: Adsorption efficiencies and mechanisms. Sep. Purif. Technol. 235, 1–9. https://doi.org/10.1016/j.seppur.2019.116152.

Jin, P., Chang, R., Liu, D., Zhao, K., Zhang, L., Ouyang, Y., 2014. Phenol degradation in an electrochemical system with TiO_2/activated carbon fiber as electrode. Elsevier 2, 1040–1047. https://doi.org/10.1016/j.jece.2014.03.023.

Khaleed, A.A., Bello, A., Dangbegnon, J.K., Momodu, D.Y., Madito, M.J., Ugbo, F.U., Akande, A.A., Dhonge, B.P., Barzegar, F., Olaniyan, O., Mwakikunga, B.W., Manyala, N., 2017. Effect of activated carbon on the enhancement of CO sensing performance of NiO. J. Alloy. Compd. 694, 155–162. https://doi.org/10.1016/j.jallcom.2016.09.310.

Kong, X., Gao, H., Song, X., Deng, Y., Zhang, Y., 2020. Adsorption of phenol on porous carbon from Toona sinensis leaves and its mechanism. Chem. Phys. Lett. 739, 137046. https://doi.org/10.1016/j.cplett.2019.137046.

Kumar, J.P., Giri, S.D., Sarkar, A., 2018. ScienceDirect Mesoporous NiO with different morphology : Synthesis, characterization and their evaluation for oxygen evolution reaction. Int. J. Hydrogen Energy 1–11. https://doi.org/10.1016/j.ijhydene.2018.06.097.

Li, H., Meng, F., Duan, W., Lin, Y., Zheng, Y., 2019a. Ecotoxicology and Environmental Safety Biodegradation of phenol in saline or hypersaline environments by bacteria: A review. Ecotoxicol. Environ. Saf. 184, 109658. https://doi.org/10.1016/j.ecoenv.2019.109658.

Li, X., Wen, H., Fu, Q., Peng, D., Yu, J., Zhang, Q., 2016. Applied Surface Science Morphology-dependent NiO modified glassy carbon electrode surface for lead (II) and cadmium (II) detection. Appl. Surf. Sci. 363, 7–12. https://doi.org/10.1016/j.apsusc.2015.12.011.

Li, Y., Du, Q., Liu, T., Sun, J., Jiao, Y., Xia, Y., Xia, L., Wang, Z., Zhang, W., Wang, K., Zhu, H., Wu, D., 2012. Equilibrium, kinetic and thermodynamic studies on the adsorption of phenol onto graphene. Mater. Res. Bull. 47, 1898–1904. https://doi.org/10.1016/j.materresbull.2012.04.021.

Li, Z., Luiz, G., Bonilla-petriciolet, A., Ben, A., 2019. Understanding the adsorption mechanism of phenol and 2-nitrophenol on a biopolymer-based biochar in single and binary systems via advanced modeling analysis 371, 1–6. https://doi.org/10.1016/j.cej.2019.04.035.

Lima, E.C., Hosseini-Bandegharaei, A., Anastopoulos, I., 2019a. Response to "Some remarks on a critical review of the estimation of the thermodynamic parameters on adsorption equilibria. Wrong use of equilibrium constant in the van't Hoff equation for calculation of thermodynamic parameters of adsorption. J. Mol. Liquids 280, 298–300. https://doi.org/10.1016/j.molliq.2019.01.160.

Lima, E.C., Hosseini-Bandegharaei, A., Moreno-Pirajᴀn, J.C., Anastopoulos, I., 2019b. A critical review of the estimation of the thermodynamic parameters on adsorption equilibria. Wrong use of equilibrium constant in the Van't Hoof equation for calculation of thermodynamic parameters of adsorption. J. Mol. Liq. 273, 425–434. https://doi.org/10.1016/j.molliq.2018.10.048.

Liu, S., Wang, J., Huang, W., Tan, X., Dong, H., Goodman, B.A., Du, H., Lei, F., Diao, K., 2019. Adsorption of phenolic compounds from water by a novel ethylenediamine rosin-based resin: Interaction models and adsorption mechanisms. Chemosphere 214, 821–829. https://doi.org/10.1016/j.chemosphere.2018.09.141.

Lu, B., Kawamoto, K., 2013. Journal of environmental chemical engineering preparation of monodispersed NiO particles in SBA-15, and its enhanced selectivity for reverse water gas shift reaction. Biochem. Pharmacol. 1, 300–309. https://doi.org/10.1016/j.jece.2013.05.008.

Luo, Z., Gao, M., Yang, S., Yang, Q., 2015. Adsorption of phenols on reduced-charge montmorillonites modified by bispyridinium dibromides: Mechanism, kinetics and thermodynamics studies. Colloids Surf., A 482, 222–230. https://doi.org/10.1016/j.colsurfa.2015.05.014.

Lütke, S.F., Igansi, A.V., Pegoraro, L., Dotto, G.L., Pinto, L.A.A., Cadaval, T.R.S., 2019. Journal of Environmental Chemical Engineering Preparation of activated carbon from black wattle bark waste and its application for phenol adsorption. J. Environ. Chem. Eng. 7, 103396. https://doi.org/10.1016/j.jece.2019.103396.

Mahmood, T., Saddique, M.T., Naeem, A., Mustafa, S., Zeb, N., Shah, K.H., Waseem, M., 2011. Kinetic and thermodynamic study of Cd (II), Co (II) and Zn (II) adsorption from aqueous solution by NiO. Chem. Eng. J. 171, 935–940. https://doi.org/10.1016/j.cej.2011.04.043.

Makrigianni, V., Giannakas, A., Deligiannakis, Y., Konstantinou, I., 2015. Journal of Environmental Chemical Engineering Adsorption of phenol and methylene blue from aqueous solutions by pyrolytic tire char : Equilibrium and kinetic studies. Biochem. Pharmacol. 3, 574–582. https://doi.org/10.1016/j.jece.2015.01.006.

Mandal, A., Das, S.K., 2019a. Phenol adsorption from wastewater using clarified sludge from basic oxygen furnace. J. Environ. Chem. Eng. 7. https://doi.org/10.1016/j.jece.2019.103259.

Mandal, A., Das, S.K., 2019b. Phenol adsorption from wastewater using clarified sludge from basic oxygen furnace. J. Environ. Chem. Eng. 7, 103259. https://doi.org/10.1016/j.jece.2019.103259.

Marques, J., Matias, T., Valente, A.J.M., Quina, M.J., 2015. Adsorption of phenol on silica aerogels using a stirred tank and a fixed bed column. Ciência & Tecnologia dos Materiais 27, 1–5. https://doi.org/10.1016/j.ctmat.2016.06.009.

Mehraban, Z., Farzaneh, F., Shafiekhani, A., 2007. Synthesis and characterization of a new organic – inorganic hybrid NiO – chlorophyll- a as optical material 29, 927–931. https://doi.org/10.1016/j.optmat.2006.02.007.

Mosallanejad, S., Dlugogorski, B.Z., Kennedy, E.M., Lomnicki, S.M., Assaf, N., Altarawneh, M., 2015. Formation of PCDD / Fs in Oxidation of 2-Chlorophenol on Neat Silica Surface. https://doi.org/10.1021/acs.est.5b04287.

Nthunya, L.N., Gutierrez, L., Derese, S., Mamba, B.B., 2019. Adsorption of phenolic compounds by polyacrylonitrile nano fi bre membranes: A pretreatment for the removal of hydrophobic bearing compounds from water. J. Environ. Chem. Eng. 7. https://doi.org/10.1016/j.jece.2019.103254.

Ouallal, H., Dehmani, Y., Moussout, H., Messaoudi, L., Azrour, M., 2019. Kinetic, isotherm and mechanism investigations of the removal of phenols from water by raw and calcined clays. Heliyon 5, e01616. https://doi.org/10.1016/J.HELIYON.2019.E01616.

Pakuła, M., Walczyk, M., Biniak, S., Świątkowski, A., 2007. Electrochemical and FTIR studies of the mutual influence of lead(II) or iron(III) and phenol on their adsorption from aqueous acid solution by modified activated carbons. Chemosphere 69, 209–219. https://doi.org/10.1016/j.chemosphere.2007.04.028.

Pirmoradi, M., Hashemian, S., Shayesteh, M.R., 2017. Kinetics and thermodynamics of cyanide removal by ZnO@NiO nanocrystals. Trans. Nonfer. Metals Soc. China 27, 1394–1403. https://doi.org/10.1016/S1003-6326(17)60160-2.

Rogozea, E.A., Petcu, A.R., Olteanu, N.L., Lazar, C.A., Cadar, D., Mihaly, M., 2017. Tandem adsorption-photodegradation activity induced by light on NiO-ZnO p–n couple modified silica nanomaterials. Mater. Sci. Semicond. Process. 57, 1–11. https://doi.org/10.1016/j.mssp.2016.10.006.

Saleh, A.M., Hassan, Y.M., Selim, S., AbdElgawad, H., 2019. NiO-nanoparticles induce reduced phytotoxic hazards in wheat (Triticum aestivum L.) grown under future climate CO 2. Chemosphere 220, 1047–1057. https://doi.org/10.1016/j.chemosphere.2019.01.023.

Santos, P.F., Neris, J.B., Heriberto, F., Luzardo, M., Velasco, F.G., Tokumoto, M.S., Serpa, R., 2019. Journal of Environmental Chemical Engineering Chemical modi fi cation of four lignocellulosic materials to improve the Pb 2 + and Ni 2 + ions adsorption in aqueous solutions. J. Environ. Chem. Eng. 7, 103363. https://doi.org/10.1016/j.jece.2019.103363.

Sheela, T., Nayaka, Y.A., 2012. Kinetics and thermodynamics of cadmium and lead ions adsorption on NiO nanoparticles. Chem. Eng. J. 191, 123–131. https://doi.org/10.1016/j.cej.2012.02.080.

Slim, K., Atoui, A., Temsah, M., 2013. Nature & Technologie Impact des rejets de margines sur la qualité des eaux du Nahr Hasbani (Sud Liban) par référence spéciale aux indices diatomiques 2–12.

Wang, P., Du, M., Zhu, H., Bao, S., Yang, T., Zou, M., 2015. Structure regulation of silica nanotubes and their adsorption behaviors for heavy metal ions: PH effect, kinetics, isotherms and mechanism. J. Hazard. Mater. 286, 533–544. https://doi.org/10.1016/j.jhazmat.2014.12.034.

Yang, H., Yu, J., Jin, H., Hyun, R., Boo, J., 2018. Applied Surface Science Improved electrochromic properties of nanoporous NiO fi lm by NiO fl ake with thickness controlled by aluminum. https://doi.org/10.1016/j.apsusc.2018.05.231

Yu, Y., Hu, Z., Wang, Y., Gao, H., 2017. Magnetic SN-functionalized diatomite for effective removals of phenols. Int. J. Miner. Process. 162, 1–5. https://doi.org/10.1016/j.minpro.2017.02.001.

Zif-, P., Dong, R., Chen, D., Li, N., Xu, Q., Li, H., He, J., Lu, J., 2020. Chemosphere Removal of phenol from aqueous solution using acid-modified. Chemosphere 239. https://doi.org/10.1016/j.chemosphere.2019.124708.